Chapter 4
Finite Element Method

The finite element method is used here to validate the analytical–numerical method presented in Chap. 3. The basic assumption and the used equations for thin plates in both the methods (ANM—the analytical–numerical method, FEM—the finite element method) are identical, but the way of solution is different. To apply a program based on the finite element method as a numerical experiment, confirming or validating the theoretical analysis or the analysis based on the analytical–numerical method, it is important to create an appropriate model. A properly chosen finite element type, a rational mesh density and appropriate boundary conditions play a significant role in obtaining the calculation results close to the reality.

In the proposed analytical–numerical method, the solution is based on the assumed deflection in the form of the sine function (3.21) in the longitudinal direction and is calculated using the numerical transition matrix method in the transverse direction. In the finite element method, the deflection function is called a shape function and it is usually assumed for each element as the first or second order polynomial. The final deflection of the whole structure is the effect of displacement of each element.

For the analysed thin-walled structures, finite shell elements seem to be the best choice. Their size and number (mesh) have to be chosen so as to map smoothly deformations. Assuming the number of elements for a dynamic buckling problem analysis, one should be aware that the map of deflection could be different than for static buckling—a number of sine halfwaves in the longitudinal direction could be greater than in the case of static load.

It seems that an application of the finite element method to replace the experiment is an easier and much cheaper option. However, please note that boundary conditions have a significant impact on the results obtained and must be the same (or similar) in all the test methods compared.

The finite element method becomes more and more popular and it represents one of the most significant developments in the history of computational methods. The finite element method has transformed much of theoretical mechanics and

T. Kubiak, *Static and Dynamic Buckling of Thin-Walled Plate Structures*,
DOI: 10.1007/978-3-319-00654-3_4,

abstract science into practical and essential tools for a multitude of technological developments which effect many facets of our life.

It is difficult to document the exact origin of the FEM but it can be said that the basic concept has evolved over a period of one hundred years or more.

The FEM theory started in the 1940s. The first formulations were developed as matrix methods for structural analysis. This led to the idea to approximate solids and Courant [4] introduced it as an assembly of triangular elements and the minimum of potential energy to torsion problems. Shortly thereafter, Clough [26] introduced the term "finite element" in the paper published together with Turner, Martin and Topp. Their paper focused on the "stiffness and deflection of complex structures". The finite element method was further enhanced during the 1960s and 1970s by such scientists as Zienkiewicz [28, 30], Hinton and Owen [10]. Zienkiewicz and Cheung [29] applied the technology to general problems described by Laplace and Poisson's equations. The major contributor among mathematicians who were developing better solution algorithms and carried out the modelling and solution of nonlinear problems was Crisfield [5]. Starting since the 1970s also Polish scientists have been concerned with the FEM—the leader was Szmelter [23, 24]. In the 1990s a rapid increase in the computing power contributed to a sudden expansion and propagated the finite element method. This method was applied to different software, which can be used in many disciplines.

Nowadays the finite element analysis is used not only for solving engineering problems but it is also used by scientists as a numerical experiment. By introducing new elements and mathematical techniques, the method has been still developing.

4.1 Dynamic Buckling

To solve the dynamic buckling problem, a response of the structure subjected to pulse load should be known. To describe the above-mentioned behaviour, the equations of motion should be solved. In the finite element method, exactly the same as in the analytical-numerical method, the differential equations of motion of the plate are derived on the basis of the Hamilton's principle (2.48):

$$\delta\Psi = \delta \int_{t_0}^{t_1} \Lambda dt = \delta \int_{t_0}^{t_1} (K - \Pi) dt = 0, \tag{4.1}$$

where K is a kinetic energy of the system and Π is a total potential energy of the system.

Similarly to the derivation presented in Sect. 2.5, the kinetic energy is:

$$K = \frac{1}{2}\rho \int_{\Omega} \{\dot{U}\}^2 d\Omega, \tag{4.2}$$

and its variation, taking into consideration identity (2.60), can be written as follows:

$$\delta K = \int_{\Omega} \rho \{\delta U\}^T \{\dot{U}\} d\Omega, \tag{4.3}$$

where {U} is a vector of the displacement function which contains the following elements: u(x,y,z,t), v(x,y,z,t), w(x,y,z,t)—functions describing displacements of a given point in three perpendicular directions in the given moment of time.

Integrating the kinetic energy variation over time, the following relation is obtained:

$$\begin{aligned} \int_{t_0}^{t_1} \delta K dt &= \int_{t_0}^{t_1} \int_{\Omega} \rho \{\delta U\}^T \{\dot{U}\} d\Omega dt \\ &= \int_{\Omega} \rho \{\delta U\}^T \{\dot{U}\} d\Omega \Big|_{t_1}^{t_2} d\Omega - \int_{t_0}^{t_1} \int_{\Omega} \rho \{\delta U\}^T \{\ddot{U}\} d\Omega dt, \end{aligned} \tag{4.4}$$

where the first term vanishes because the displacement variation $\{\delta U\}$ equals zero for $t = t_0$ and $t = t_1$.

The total potential energy variation $\delta\Pi$ can be written in the form:

$$\delta \Pi = \delta Q - \delta W, \tag{4.5}$$

where δQ is a variation of the internal elastic strain energy:

$$\delta Q = \int_{\Omega} \{\delta \varepsilon\}^T \{\sigma\} d\Omega, \tag{4.6}$$

and δW is a variation of work of the external forces $\{F\}$:

$$\delta W = \int_{\Omega} \{\delta U\} \{F\} d\Omega. \tag{4.7}$$

Substituting (4.4) and (4.5) into (4.1), the Hamilton's principle can be written in the form:

$$\int_{t_0}^{t_1} \int_{\Omega} [\rho \{\delta U\}^T \{\ddot{U}\} - \{\delta \varepsilon\}^T \{\sigma\} + \{\delta U\}^T \{F\}] d\Omega dt = 0. \tag{4.8}$$

In the finite element method, the displacement {U} for any point of the structure should be related to the nodal displacements {u} using an arbitrary assumed shape function [N_u]:

$$\{U\} = [N_u]\{u\}. \tag{4.9}$$

The shape function of the element applied to discretize the structure is also used to express:

- strains $\{\varepsilon\}$ by the vector of nodal displacements $\{\mathrm{u}\}$ and derivatives of the shape function called the geometrical matrix $[B_\mathrm{u}]$:

$$\{\varepsilon\} = [D][N_u]\{u\} = [B_u]\{u\}, \tag{4.10}$$

where:

$$[D] = \begin{bmatrix} \partial_x & 0 & 0 \\ 0 & \partial_y & 0 \\ 0 & 0 & \partial_z \\ 0 & \partial_z & \partial_y \\ \partial_z & 0 & \partial_x \\ \partial_y & \partial_x & 0 \end{bmatrix}, \partial_x = \frac{\partial}{\partial x}, \partial_y = \frac{\partial}{\partial y}, \partial_z = \frac{\partial}{\partial z}, \tag{4.11}$$

- stress $\{\sigma\}$ by the vector of nodal displacements $\{\mathrm{u}\}$, the geometrical matrix $[B_\mathrm{u}]$ and the material properties matrix [Q]:

$$\{\sigma\} = [Q]\{\varepsilon\} = [Q][B_u]\{u\}. \tag{4.12}$$

Substituting (4.9)–(4.12) to the Hamilton's principle, i.e., to (4.8), the following form is obtained:

$$\{\delta u\}^T \int_\Omega [\rho[N_u]^T[N_u]d\Omega\{\ddot{u}\} - \{\delta u\}^T \int_\Omega [B]^T[Q][B]d\Omega\{u\} + \{\delta u\}^T \int_\Omega [N_u]^T\{F\}d\Omega = 0, \tag{4.13}$$

where the integration over time is omitted for simplicity. The integration requires a numerical procedure which is carried out in discretized moments with the established time step of integration. The Newmark method [1, 2] is a very popular procedure also used in the ANSYS software.

Equation (4.13) must be satisfied for any variation of displacements (weight functions) in any moment of time from t_0 to t_1 and fulfil the relevant boundary conditions. This is a weak (variation) formulation of finite element method equations, where the generalized Galerkin method [3, 21, 27] has been used. Equating to zero the coefficients standing by the variations of displacements, the following equation is obtained in the matrix form:

$$\{\mathrm{P}\} = [\mathrm{M}] \cdot \{\ddot{\mathrm{u}}\} + [\mathrm{K}] \cdot \{\mathrm{u}\}, \tag{4.14}$$

where:

$[M] = \int_{\Omega} [\rho [N_u]^T [N_u] d\Omega$ is a mass matrix of the structure,

$[K] = \int_{\Omega} [B]^T [Q][B] d\Omega$ is a structural stiffness matrix,

$\{P\} = \int_{\Omega} [N_u]^T \{F\} d\Omega$ is a vector of generalized nodal forces.

After replacing the time derivatives of displacements $\{\ddot{\mathrm{u}}\}$ by the displacement differences $\{\mathrm{u}\}$ in successive discrete moments of time t, a new static equilibrium equation for the each time step is obtained. It contains the inertia forces $[\mathrm{M}]\{\ddot{\mathrm{u}}\}$ and, therefore, it is possible to apply the algorithms used in the static analysis. The time integration in the ANSYS program is conducted using the Newmark method [2] and a solution to equations in successive time steps is obtained with the Newton-Raphson algorithm [7].

Equation (4.14) does not take into account the material-dependent damping, which according to [13] can be neglected in the dynamic buckling analysis of thin-walled structures subjected to uniform compression. However, the recent paper [14] has shown a significant role of dumping in the case when the viscoelastic material model with the strain rate effect is taken into account and/or the analysed structures are subjected to torsion or combined load (bending and torsion). In this case, the damping related to the speed of displacement should be added to (4.14), which takes the form:

$$\{\mathrm{P}\}=[\mathrm{M}] \times \{\ddot{\mathrm{u}}\}+[\mathrm{C}] \times \{\dot{\mathrm{u}}\}+[\mathrm{K}] \times \{\mathrm{u}\}, \tag{4.15}$$

where $[\mathrm{C}]$ is a damping matrix, which according to the ANSYS manual [1] depends on the mass matrix of structures $[\mathrm{M}]$ and the structural stiffness matrix $[\mathrm{K}]$. The relation is as follows:

$$[\mathrm{C}] = \alpha[\mathrm{M}] + \beta[\mathrm{K}], \tag{4.16}$$

where α and β are damping coefficients specified as decimal numbers. The values of α and β [1] are not generally known directly, but can be calculated from the modal damping ratio ψ_{i}, which is the ratio of actual damping to critical damping for the i-th mode of vibration. Denoting the natural circular frequency of the i-th mode by ω_{i}, the coefficients α and β satisfy the relation:

$$\psi_i = \frac{\alpha}{2\omega_i} + \frac{\beta\omega_i}{2}. \tag{4.17}$$

In many practical structural problems, the alpha damping (or the *mass* damping) may be ignored ($\alpha = 0$). In such cases, the beta damping β can be evaluated from known values of ψ_{i} and ω_{i} as:

$$\beta = \frac{2\psi_i}{\omega_i}, \tag{4.18}$$

and then the damping matrix can be expressed as follows:

$$[\mathrm{C}] = \beta[\mathrm{K}]. \tag{4.19}$$

It should be noted that (in the ANSYS software [1]):

- in the transient harmonic response analysis, the *material-dependent* damping can be only specified as the beta damping (β), using the command defining material properties;
- only one β can be input in each load step, so the most dominant frequency ω_i should be chosen to calculate the beta damping coefficient.

The dynamic buckling analysis or the response analysis of the structure subjected to pulse load requires the following assumptions:

- shape and amplitude of imperfection,
- shape and amplitude (defined as DLF) of pulse load,
- time of pulse duration.

Therefore, before attempting to solve the dynamic buckling problem, the eigenbuckling solution (Sect. 4.3) should be achieved to determine the critical load and the corresponding buckling mode. The buckling mode corresponding to the lowest critical load is used to map the shape of geometrical imperfections with the assumed amplitude, usually equal to 1/100 thickness of the plate or the wall of the column. The modal analysis (Sect. 4.4) is performed to calculate the natural frequencies of the structure which are used to determine the duration of pulse load. The pulse duration T_p is usually assumed as a half or one period of the natural vibration T.

The above discussed analysis has been carried out using the ANSYS software [1] based on the finite element method.

4.2 Nonlinear Buckling Analysis

A nonlinear buckling analysis is in fact a static analysis with geometrical nonlinearities (large deflections included into the analysis). This kind of analysis allows one to find the buckling load, to analyse the postbuckling behaviour of structures, to estimate the load carrying capacity and a mode of failure.

For the structures which are subject to perfectly in-plane load (uniformly compressed plates or columns), small out-of-plane perturbations are necessary to initiate the buckling response. These perturbations can be applied as a modest temporary force or a specified displacement. It should be noted that the failure load is very sensitive to initial imperfections, therefore, these initial perturbations should be as small as possible. Usually, at the beginning the eigenbuckling

analysis is performed to calculate the buckling load and the corresponding buckling mode. The shape of the buckling mode allows one to predict the place where the force as the initial perturbation should be applied. In the case of the initial displacement, the buckling mode is used as the perturbation to map it into the finite element model.

In other cases of load, i.e., out-of-plane load or in-plane load but with eccentricity, the initial perturbation is not necessary.

Having the proper model, the following equation is solved:

$$[\overline{\mathrm{K}}] \cdot \{\mathrm{u}\} = \{\mathrm{P}\}, \tag{4.20}$$

where the stiffness matrix $[\overline{\mathrm{K}}]$ is dependent on the nodal displacement, which means that the static problem is no longer geometrically linear—it is a nonlinear problem (in the ANSYS software, the nonlinear geometry procedure should be switched on). From the theoretical point of view, this nonlinear static problem can be treated as a large strain or large rotation problem. In the first case (i.e., large strain), strains in the material exceed more than a few percent—it usually happens when a hyperelastic problem or an elastic-plastic problem is solved. In the second case (large rotation), rotations are large and mechanical strains are small. The second case describes situations similar to the postbuckling analysis in an elastic range, especially when the deflections of thin-walled structures are less than 5 thicknesses of the plate or girder wall—the results are similar to the one obtained from the analytical-numerical method described in Chap. 3.

The stiffness matrix $[\overline{\mathrm{K}}]$ should be treated as the tangent stiffness matrix for the i-th increment of displacement and it is usually denoted as $[K_i^T]$. Depending on the type of geometric nonlinearity, the tangent stiffness matrix $[K_i^T]$ and the vector of restoring forces for the i-th iteration $\{P_i^r\}$ are formulated in a different way. According to the notation used in (4.20), the vector of restoring force (at each iteration) is a part of the vector {P}, which can be expressed as:

$$\{P\} = \{P^a\} - \{P_i^r\}, \tag{4.21}$$

where $\{P^{\mathrm{a}}\}$ is a vector of applied nodal forces.

For a large strain problem formulation, the tangent stiffness matrix is as follows:

$$[K_i^T] = [K_i] + \int_{\Omega} [G_i]^T [\tau_i][G_i] d\Omega, \tag{4.22}$$

where $[\mathrm{K_i}]$ is an elemental stiffness matrix (well known from the static linear problem formulation), $[\mathrm{G_i}]$ is a matrix of shape function derivatives and $[\tau_{\mathrm{i}}]$ is a matrix of the current Cauchy (true) stresses $\{\sigma_{\mathrm{i}}\}$.

The vector of restoring forces corresponding to the element internal loads for the i-th iteration $\{P_i^r\}$ in the large strain problem formulation is:

$$\left\{P_i^r\right\} = \int_{\Omega} [B_i]\{\sigma_i\}\mathrm{d}\Omega. \tag{4.23}$$

For the large rotation problem formulation, the tangent stiffness matrix is as follows:

$$\left[K_i^T\right] = \int_{\Omega} [T_n]^T [B_V]^T [D][B_V][T_n] d\Omega, \tag{4.24a}$$

where $[B_v]$ is a small strain-displacement relationship in the original (virgin—non-deformed) element coordinate system and $[T_n]$ is an orthogonal transformation relating the original element coordinates to the converted (or rotated) element coordinates. The rotated element coordinate system differs from the original coordinate system by the amount of rigid body rotation. Hence, the transformation matrix $[T_n]$ is computed by separating the rigid body rotation from the total deformation $\{u_n\}$ using the polar decomposition theorem (the deformation of the object could be decomposed as the rotation plus stretching).

The vector of restoring forces for the i-th iteration $\left\{P_i^r\right\}$ in the large rotation problem formulation is:

$$\left\{P_i^r\right\} = \int_{\Omega} [T_n]^T [B_V]^T [D][B_V]\{u_d\} d\Omega, \tag{4.24b}$$

where $\{u_d\}$ is the element deformation which causes straining [1].

The Newton-Raphson method, which is graphically presented in Fig. 4.1, is most popular for solving nonlinear problems with the iterative method. For a single iteration, (4.20) has the form [2]:

$$\left[K_i^T\right]\{\Delta u_i\} = \{P^a\} - \left\{P_i^r\right\}, \tag{4.25}$$

where the increment of displacement $\{\Delta u_i\}$ is assumed and fulfils the following relation:

$$\{u_{i+1}\} = \{u_i\} + \{\Delta u_i\}. \tag{4.26}$$

The general algorithm for the Newton-Raphson procedure (Fig. 4.1) can be described as the general algorithm and proceeds as follows:

1. Assume an initial displacement vector $\{u_0\}$. In the first time step, the initial displacement vector is assumed as zero $\{u_0\} = \{0\}$ and for next time steps, $\{u_0\}$ is assumed as the displacement vector from the previous time step converged solution.
2. Compute the updated tangent matrix $[K_i^T]$ and the restoring load vector $\left\{P_i^r\right\}$ for the displacement vector $\{u_i\}$ for the i-th iteration.
3. Calculate a vector of the displacement increment $\{\Delta u_i\}$ from (4.25).
4. Find the next approximation $\{u_{i+1}\}$ from (4.26).

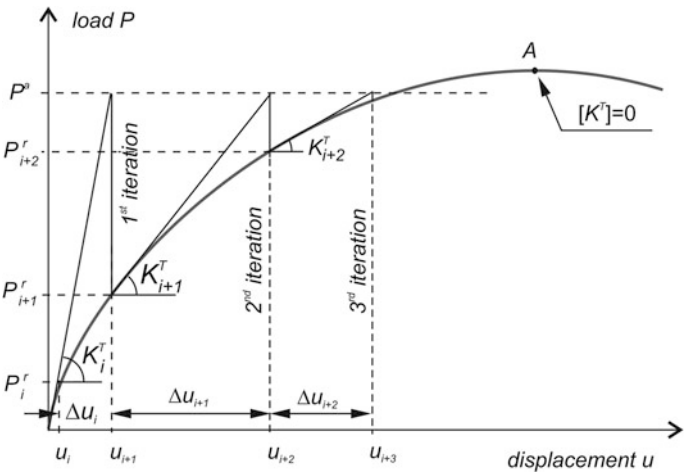

Fig. 4.1 Graphical representation of the Newton-Raphson algorithm

5. Repeat steps 2–4 until a convergence is obtained.

In practice, more than one iteration is needed to obtain a converged solution. In order to improve and speed up the procedure, the incremental Newton-Raphson procedure (Fig. 4.2a) or the initial-stiffness Newton-Raphson procedure (Fig. 4.2b) is used. In the incremental procedure, the applied load is divided in a few substeps (Fig. 4.2a). Using the initial-stiffness Newton-Raphson procedure, the tangent stiffness matrices are the same during each iteration, which requires fewer matrix reformulations and inversions than in the full Newton-Raphson procedure. It should be also mentioned that due to numerous iterations, the initial-stiffness Newton-Raphson procedure converges more slowly than the full Newton-Raphson procedure.

The main disadvantage of the Newton-Raphson method is such that it stops the procedure when the determinant of the tangent stiffness matrix is equal to zero (point A in Fig. 4.1).

Therefore, the arc-length technique (Riks method) is used. The Riks method [22] is suitable for nonlinear static equilibrium solutions to unstable problems, allows for finding the load carrying capacity and for analysing a failure mode. The arc-length method in the ANSYS software uses the explicit spherical iterations to maintain the orthogonality between the arc-length radius and orthogonal directions as described by Forde and Stiemer [6]. A graphical representation is shown in Fig. 4.3. It is assumed that all load magnitudes in (4.25) are controlled by the total load factor λ, which is in the range $\langle -1,1 \rangle$. Then, in the arc-length method, (4.25) has the form:

$$\left[K_i^T\right]\{\Delta u_i\} = \lambda\{P^a\} - \left\{P_i^r\right\}. \tag{4.27}$$

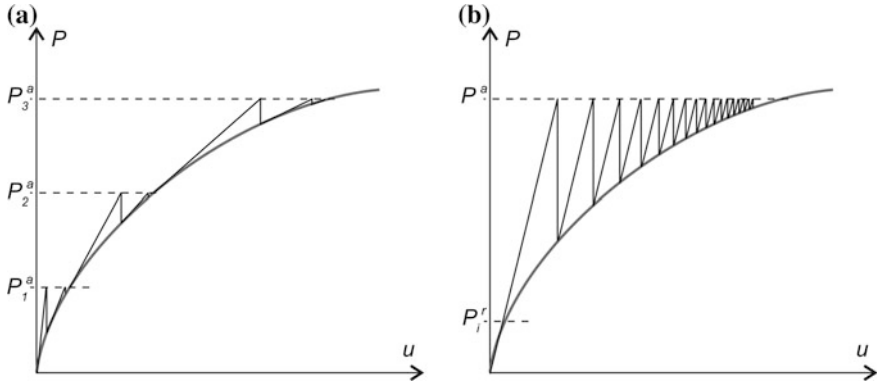

Fig. 4.2 Graphical representation of the incremental Newton-Raphson procedure (**a**) and the initial-stiffness Newton-Raphson procedure (**b**)

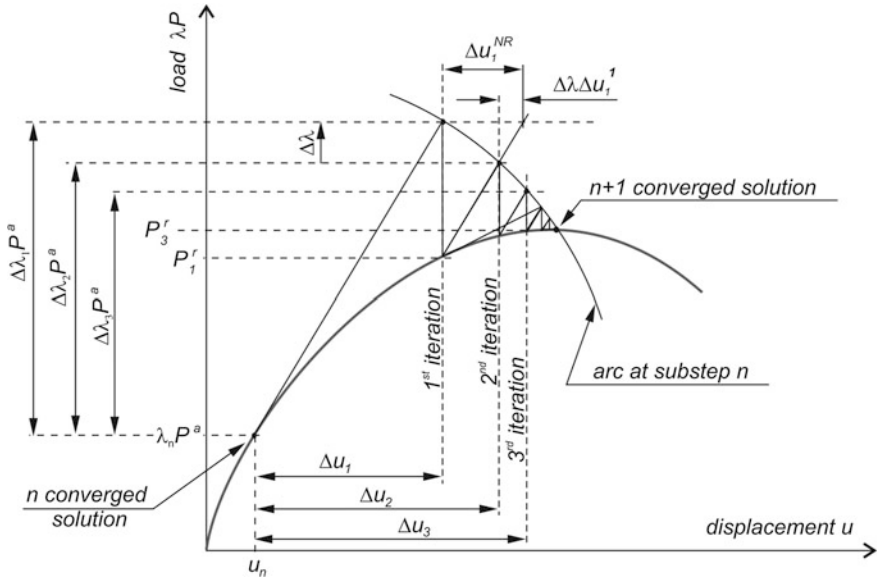

Fig. 4.3 Graphical representation of the arc-length method

Equation (4.27) in the incremental form for the intermediary step (i.e., at the substep n and the iteration i) has the following form:

$$\left[K_i^T\right]\{\Delta u_i\} - \Delta\lambda\{P^a\} = (\lambda_n + \lambda_i)\{P^a\} - \left\{P_i^r\right\}, \tag{4.28}$$

where $\Delta\lambda$ is an incremental load factor (Fig. 4.3).

On the basis of (4.28), the relation describing the vector of incremental displacement $\{\Delta u_i\}$ can be written as follows:

$$\{\Delta u_i\} = \Delta\lambda\{\Delta u_i^1\} + \{\Delta u_i^{NR}\}, \tag{4.29}$$

where $\{\Delta u_i^1\}$ is the vector of incremental displacement corresponding to a unit load factor and $\{\Delta u_i^{NR}\}$ is the vector of incremental displacement taken from the conventional Newton-Raphson method (4.25). Both the vectors of incremental displacement are defined by:

$$\{\Delta u_i^1\} = [K_i^T]^{-1}\{P^a\}, \tag{4.30}$$

$$\{\Delta u_i^{NR}\} = [K_i^T]^{-1}\left((\lambda_n + \lambda_i)\{P^a\} - \{P_i^n\}\right), \tag{4.31}$$

and both of them should be determined in each arc-length iteration. Then, the incremental load factor $\Delta\lambda$ is determined by the arc-length l_i equation, which at the i-th iteration can be written as (Fig. 4.3):

$$l_i^2 = \Delta\lambda_i^2 + \beta^2\{\Delta u_n\}^T\{\Delta u_n\}, \tag{4.32}$$

where β is a scaling factor, Δu_n is a sum of all the displacement increments Δu_i of this iteration.

Finally, the arc-length load increment factor $\Delta\lambda$ is determined by the formula:

$$\Delta\lambda = \frac{r_i - \{\Delta u_n\}^T\{\Delta u_i^{NR}\}}{\beta^2\lambda_i + \{\Delta u_n\}^T\{\Delta u_i^1\}}, \tag{4.33}$$

where r_i is a residual parameter (a scalar) obtained by multiplication of the normal and tangential vectors.

The arc-length method has also disadvantages and the main one is the requirement to adjust the arc-length radius by trial-and-error in a series of manually directed reanalyses.

4.3 Linear Static Buckling Analysis

The linear buckling analysis of the structure subjected to static load is called the eigenbuckling problem. The eigenbuckling is used for bifurcation buckling of the linearized model of elastic stability. This type of analysis allows for calculating the buckling load with the corresponding buckling mode. The term "eigenbuckling" comes from the method of formulation of the problem, so the eigenvalue equation for buckling problem take the form:

$$([K] + \lambda_i[S])\{\psi\}_i = \{0\}, \tag{4.34}$$

where [K] is a structural stiffness matrix, [S] is a stress stiffness matrix, λ_i is the i-th eigenvalue and ψ_i is the i-th eigenvector of displacement.

It should be added that the eigenvalue λ_i is a load multiplier that allows one to find the i-th buckling load. The i-th buckling load is calculated as the applied load multiplied by the i-th eigenvalue λ_i.

The stress stiffness matrix [S] is determined in the static analysis. It means that before the eigenbuckling analysis, the static analysis should be performed.

Equality (4.34) is satisfied if the eigenvector of displacement is equal to zero or if the determinant of the term in brackets is equal to zero. The $\{\psi\}_i = 0$—a trivial solution to (4.34)—is out of interest. It means that the structure does not change the "shape"—the structure remains in the initial state of equilibrium. Thus, the term in brackets in (4.34) gives the following solution:

$$|[K] + \lambda_i[S]| = 0. \tag{4.35}$$

Equation (4.35) represents the eigenvalue problem which allows for finding n values of the buckling load multiplier λ and the corresponding buckling mode shape. The number n depends on the number of DOFs assumed in the finite element model (n = DOF number).

It should be noted that in the FEM software as well as in the ANSYS software, the eigenvectors are normalized so that the largest component is 1.0. Thus, stresses may be interpreted only as a distribution of relative stresses.

4.4 Modal Analysis

The modal analysis is used to find natural frequencies and the corresponding modal modes. The solution to the problem is based on equation of motion (4.14) for an undamped system in which the left-hand side is equal to zero and which can be expressed in the form:

$$[\mathrm{M}] \cdot \{\ddot{\mathrm{u}}\} + [\mathrm{K}] \cdot \{\mathrm{u}\} = \{0\}. \tag{4.36}$$

The vector of the nodal displacement for free vibrations of a linear system is assumed as a harmonic of the following form:

$$\mathrm{u} = \{\phi\}_i \cos \omega_i \mathrm{t}, \tag{4.37}$$

where $\{\phi\}_i$ is an eigenvector representing the mode shape of the i-th natural frequency, ω_i is the i-th natural circular frequency, and t denotes time.

Substituting the assumed vector of the nodal displacement (4.37) into equation of motion (4.36), the following relation is obtained:

$$\left(-\omega_i^2[M] + [K]\right)\{\phi\}_i = \{0\}. \tag{4.38}$$

Equality (4.38) is satisfied if the eigenvector representing the mode shape $\{\phi\}_i$ is equal to zero or if the determinant of the term in brackets is equal to zero. The

$\{\phi\}_i = 0$ is a trivial solution to (4.38), which is out of interest. Thus, the following solution is obtained:

$$\left|-\omega_i^2[M] + [K]\right| = 0. \tag{4.39}$$

Equation (4.39) represents the eigenvalue problem, which allows for finding n values of natural circular frequencies ω and the corresponding eigenvectors, which allow one to describe the modal mode. The number n equals to the number of DOFs assumed in the finite element model.

4.5 Element Type

The most suitable element for plated thin-walled structures is a shell element. An exemplary four-node shell element with six degrees of freedom at each node is presented in Fig. 4.4. In the case when the layered plate is modelled, a multilayer shell element can be used for which the material properties as well as orientations are defined for each layer.

Shell elements have only five independent degrees of freedom at each node (three perpendicular displacements and two rotations around the axis lying in the plane of the element). The sixth degree of freedom (a rotation around the axis normal to the plane of element) is not independent. Two different and possible shapes of displacements (a relation between rotations θ_z for each node in one element) are presented in Fig. 4.5. The relations between rotations are controlled for each element using the concept proposed by MacNeal and Harder [20].

The shape function for the presented element is assumed as the first order (linear) polynomial and has the following form:

$$N_e = \frac{1}{4}[u_I(1-s)(1-t) + u_J(1+s)(1-t) + u_K(1+s)(1+t) + u_L(1-s)(1+t)]. \tag{4.40}$$

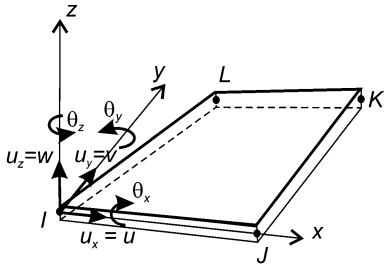

Fig. 4.4 Quadrilateral, four nodal shell element [1]

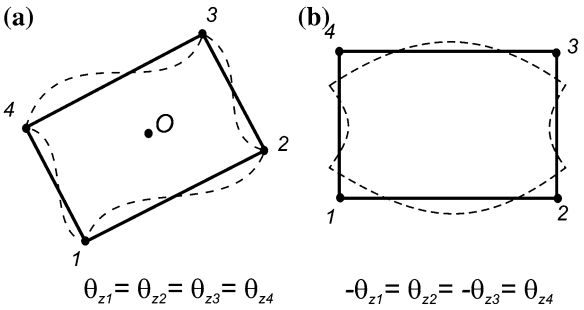

Fig. 4.5 Possible rotation around the axis normal to the plane of the element [1]. Spurious Mode (**a**), Hourglass Mode (**b**)

4.6 Discretization

As is very well known, the number of elements has a significant influence on the results of calculation. In all cases of the FEM calculations presented in this book, the number of elements has been assumed on the basis of experience [11, 12, 15–18]. The model discretized with a not enough number of elements is stiffer than the real structure and the results are not correct. The opposite case, i.e., too many elements used for discretization, leads to time-consuming calculations. The number of elements (the density of elements) should be chosen on the basis of the solution convergence analysis. An exemplary analysis of the solution convergence for the buckling problem is presented in Table 4.1. This analysis was performed for a square plate subjected to uniform compression. The plate thickness defined as thickness to length of the plate is equal to 1/100. The plate was simply supported on loaded edges and fixed on longitudinal edges. The use of four-node shell elements to represent the form of buckling needs the plate to be meshed into at least five elements along each sine halfwave. An increase in the number of elements increases the number of nodes and degrees of freedom for the model, which allows for mapping the highest buckling mode (the mode with more than one halfwave of sine). The 10 lowest buckling loads with the corresponding modes for different mesh densities (the number of elements in the longitudinal and transverse direction) have been determined and presented in Table 4.1.

It is well known that for the isotropic square plate fixed on the longitudinal edges and simply supported on the loaded edges, the mode corresponding to the lowest buckling has two halfwaves in the longitudinal direction ($m = 2$) and one halfwave in the transverse direction ($n = 1$). As presented in the exemplary results of calculation, the worst assumed mesh density (three elements in the longitudinal and transverse directions) did not give proper results—the lowest value was obtained for the buckling mode with one halfwave in both directions ($m = 1$, $n = 1$). Some buckling modes, which were found for a denser mesh, were not determined for the 3 by 3 elements mesh. An increase in the number of elements (from 3×3 to 5×5) by almost three times allows one to determine the same buckling mode (i.e., $m = 2$, $n = 1$) as is well known from the literature [25], but still not all buckling modes could be found (Table 4.1). Once again, an increased

Table 4.1 Influence of the mesh density on the buckling load [kN]

Mode[a]		3 × 3	Change (%)[b]	5 × 5	Change (%)[b]	10 × 10	Change (%)[b]	20 × 20	Change (%)[b]	40 × 40
m	*n*									
2	1	28.2	40	16.8	14	14.5	3	14.0	1	13.9
1	1	26.0	30	18.1	11	16.1	3	15.7	1	15.5
3	1	–		39.8	39	24.3	9	22.1	2	21.6
4	1	–		164.8	74	43.1	18	35.5	4	34.0
3	2	–		–		44.7	8	41.3	2	40.5
2	2	719.3	91	62.8	28	45.2	7	42.2	2	41.5
4	2	–		190.9	69	60.0	14	51.5	3	49.7
5	1	–		–		76.6	29	54.3	7	50.4
5	2	–		–		91.9	25	68.8	6	64.7
6	1	–		–		–		79.4	11	71.1

[a] *m, n*—number of halfwaves in longitudinal and transverse directions, correspondingly
[b] percentage change in the critical value relative to the result for the worse mesh

number of elements in the longitudinal and transverse directions (10 × 10) has resulted in further improvement of buckling loads value—the percentage change of the buckling load corresponding to all determined modes is in the range from 11 to 74 %. A 10 × 10 mesh allows one to determine nine from ten first modes which could be found using a denser mesh. A further increase in the number of elements (20 × 20) allows one to find all first ten modes and leads to a percentage change of the buckling load from 3 to 29 % in comparison with a less dense mesh. If the criterion that the improvement of the result by less than 5 % does not require a further increase of the mesh density is assumed, then it can be said that the appointment of the two lowest critical power density distributions of 20 × 20 is correct. Moreover, it can be noticed that the mesh improvement to receive 40 by 40 elements does not change first seven buckling loads by more than 5 % compared to the 20 × 20 mesh.

To be sure that the mesh density is correct not only for the static buckling analysis but also for the dynamic buckling analysis, the dynamic response for different amplitudes of the rectangular pulse load was checked. It is necessary because during and after the pulse load duration, the shape of deflection can change rapidly with an increase in the pulse amplitude.

For exemplary calculations, a rectangular pulse shape was chosen. The pulse duration is assumed to be equal to the period of natural vibrations for the analysed plate $T_p = T$. Two different mesh densities were considered—it was a 5 × 5 element mesh and a 20 × 20 element mesh in two orthogonal directions. Because the first modal mode has one halfwave of sine in the longitudinal direction ($m = 1$) and the first buckling mode has two halfwaves of sine, it was decided to conduct the analysis for both mode cases. For the case denoted as $m = 1$, the initial imperfection corresponded to the modal mode with the amplitude equal to 1/100 of the plate thickness, the pulse duration was equal to the period of natural vibrations for the mode with one halfwave of sine. The dynamic load factor DLF was

calculated as the pulse amplitude divided by the buckling load for the mode $m = 1$ of the value corresponding to the assumed mesh density (Table 4.1). The similar assumptions were made for the case denoted as $m = 2$: the amplitude of initial imperfections equals 1/100 of the plate thickness and the initial imperfection shape corresponded to the first buckling mode ($m = 2$), the pulse duration equalled the period of natural vibrations for the mode $m = 2$ and the dynamic load factor DLF determined as the pulse amplitude divided by the buckling load for the mode $m = 2$.

The results are shown in Fig. 4.6 in the form of curves presenting the dependence of the maximum dimensionless deflection ξ as a function of the dynamic load factor DLF (Dynamic Load Factor—amplitude of the pulse load to the static buckling load). For the case denoted as $m = 2$, the curves ξ(DLF) presented in Fig. 4.6 for both mesh densities 5×5 and 20×20 are relatively close to each over. However, for the case of $m = 1$, the curves ξ(DLF) for both densities of the mesh taken into account overlap only for DLF ≤ 1.6 but for higher DLF values, the curves ξ(DLF) differ—see Fig. 4.6.

If the nodal displacement for $DLF = 3$ and for two mesh densities is compared (Fig. 4.7), it is clear that the model divided into a smaller number of elements (Fig. 4.7a) cannot present smoothly the shape of the deformed plate.

This example shows that the assumption of the finite element mesh density chosen in such a way that each square part of the column wall or the single plate is divided into 20×20 elements is correct and it should yield proper results.

4.7 Load and Boundary Conditions

Boundary conditions assumed on loaded edges depend on the analysed structure (a plate, a beam-column with an open and closed cross-section) and a type of load (uniform compression, eccentricity compression, pure bending). To obtain the results of the FEM analysis as close as possible to the experimental test or the numerical analysis made with another method, the assumed boundary conditions should be defined the same or similar in both compared tests/methods.

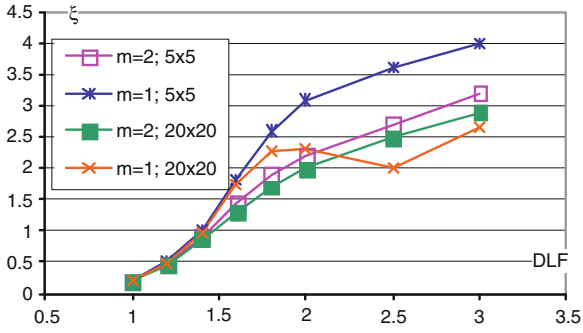

Fig. 4.6 Nondimensional deflection vs. the dynamic load factor for different elements sizes and buckling modes

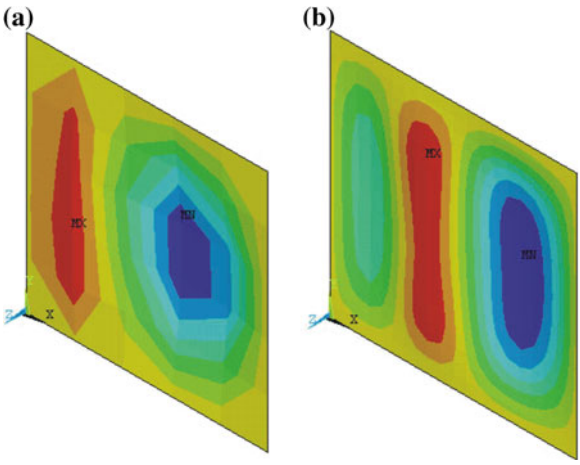

Fig. 4.7 Map of deflection for $DLF = 3$ and the element mesh equal to 5×5 (**a**) or 20×20 (**b**)

The boundary conditions in the FEM are determined defining nodal generalized displacements (displacements, rotations) and/or a coupled displacement for a group of nodes.

For all the analysed plates, the boundary conditions on longitudinal (unloaded) edges are set as follows (notation according to Fig. 4.8):

- simple supported: $v =$ constant and $w = 0$,
- clamped: $v =$ constant and $w = 0$ and $\theta_x = 0$,
- free edge—any constrains on the nodal displacement not set.

The boundary conditions set on loaded edges correspond to simply supported and, depending on a type of load, they are as follows:

- uniform compression: $u =$ constant and $w = 0$,
- pure in-plane bending or eccentricity compression: $\theta_z =$ constant and $w = 0$ and for one edge node lying on the neutral axis (middle node) $u = 0$.

To determine only the local buckling mode for the compressed column or girder, the boundary conditions assumed on loaded edges on the girder wall can be exactly the same as for the simply supported plate under uniform compression. In the case of pure bending or eccentricity compression of beam-columns or girders, the planes on which the loaded edges lie can rotate due to the assumed type of loading. Taking the above into account, the proper boundary condition should be considered. An exemplary way of finding the proper boundary condition for the girder with a closed cross-section is presented below [19].

The boundary conditions assumed in the analytical-numerical method in the prebuckling state in comparison to the buckling and postbuckling state are different. The above-mentioned differences were noticed and used in the FEM modelling of the compressed tube by Guarracino [8, 9]. It should be noted that also in the case of the girder with a closed cross-section subjected to pure bending, the boundary conditions in prebuckling and postbuckling states are different. That was the reason

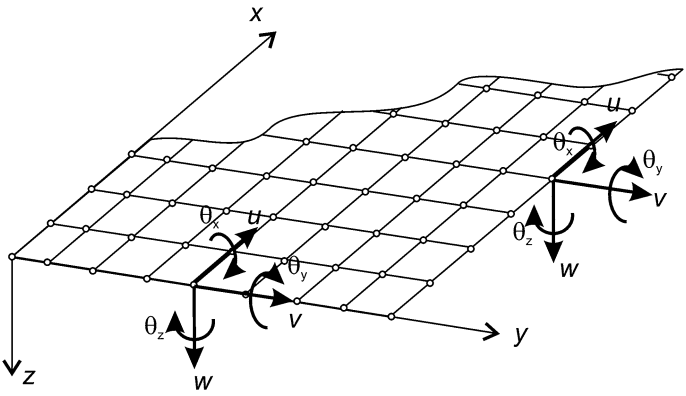

Fig. 4.8 Nodal displacement for the plate

to suggest and test different boundary condition models [18]. Three of them, denoted as **A**, **B** and **C,** respectively, are presented in Figs. 4.9, 4.10 and 4.11.

The proposed type **A** of boundary conditions (Fig. 4.9) ensures that the loaded edges remain straight—the nodal displacement for all nodes lying on wall edges in the direction normal to the wall was set to zero. In the next boundary condition model (type B—Fig. 4.10), the beam element was additionally applied as a stiffener on all loaded edges. The added stiffeners—the beam element—should be rigid for bending, compression and tension (the edges on which beam elements lie should stay straight after loading) and flexible for twisting (allow to rotate the plate or the wall around ending edges). To fulfil rigidity, the height of the beam is assumed to be 10 times greater than the thickness of the plate. To fulfil flexibility

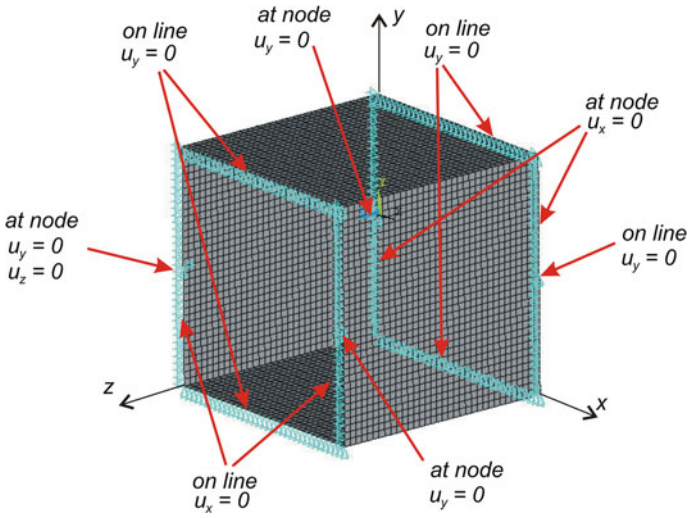

Fig. 4.9 Type **A** of boundary conditions—zero value of the nodal displacement

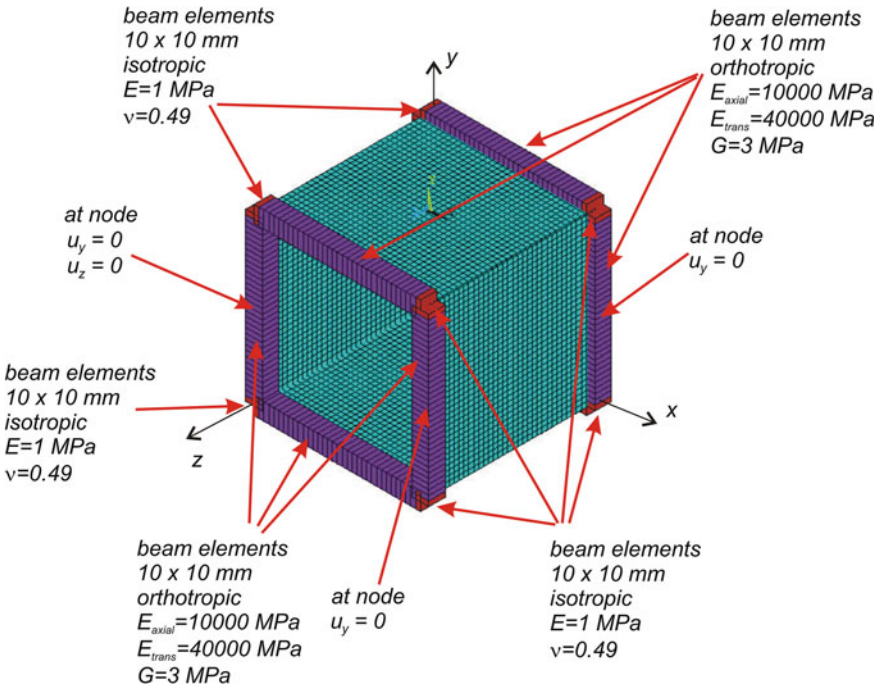

Fig. 4.10 Type **B** of boundary conditions—zero value of the nodal displacement and beam stiffeners

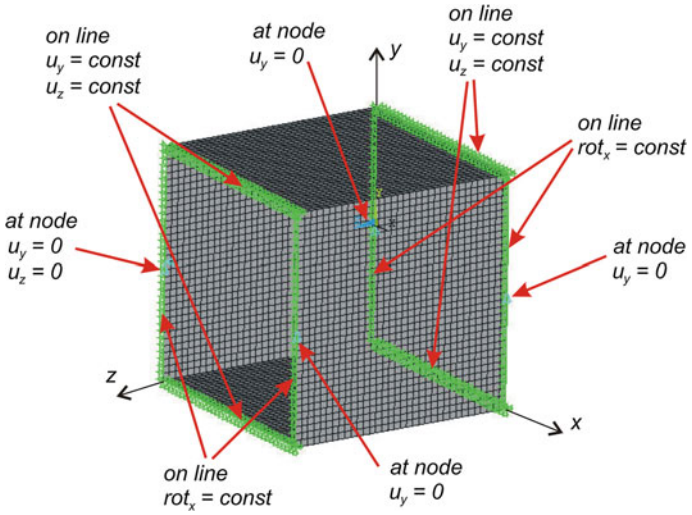

Fig. 4.11 Type **C** of boundary conditions—zero value of the nodal displacement and coupled boundary conditions

allowing rotations, the orthotropic material properties with the low Kirchhoff's modulus were assumed. Additionally, beam elements lying near the corner (red elements—Fig. 4.10) have much lower stiffness, so the corners will be not too stiff and will allow changes in the shape of the cross section as it happens during bending.

In the last presented here model of the assumed boundary conditions—type C (Fig. 4.11), not only zero value of the displacement but also of the coupled degree of freedom was used. For walls of girders or beam-columns which are uniformly compressed or tensioned, for all nodes lying on edges in longitudinal and normal to the wall directions, the constant displacement was set. For all nodes lying on the edges of the wall which were subjected to in-plane bending, the constant displacement in normal to the wall direction and a constant rotation around the bending neutral axis was set.

All three above-mentioned types of boundary conditions were tested in static buckling and dynamic responses during the pulse load numerical analysis. To choose "the proper" boundary conditions, a criterion was used which aimed at obtaining the results of calculations as closest as possible in both the methods—the FEM and the ANM.

Buckling modes and buckling loads for girders with a square cross-section made of a composite material with the volume fibre fraction $f = 0.5$ are presented in Fig. 4.12 and Table 4.2. The nondimensional value of the critical bending moment M_{cr}/M_{crANM} is determined by dividing the FEM critical moment by the critical moment obtained from the analytical-numerical method.

The assumed criterion and the results (Table 4.2) obtained from the stability analysis have shown that all the proposed boundary conditions can be considered to be correct—the differences between the results are less than 1 %. In all the analysed cases the buckling modes were the same (Fig. 4.12). None of the proposed models of boundary conditions could be disqualified. Therefore, for each of them, the analysis of the dynamic response to the pulse bending moment was carried out. A rectangular pulse with duration equal to the period of natural vibration of the analysed structure was assumed. The results are presented

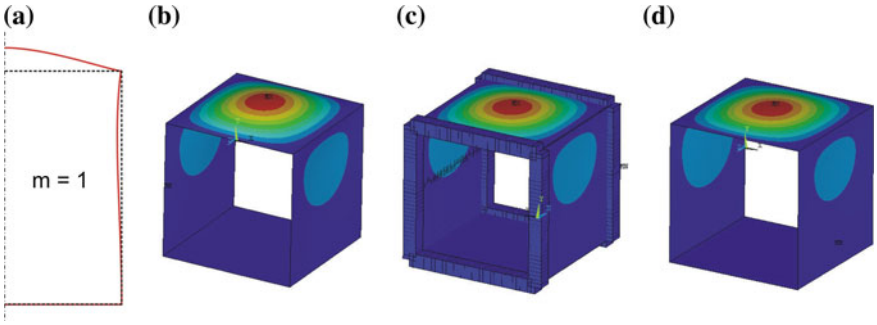

Fig. 4.12 Buckling mode obtained from the analytical-numerical method (**a**) and the finite element method with boundary conditions of types **A** (**b**), **B** (**c**) and **C** (**d**)

Table 4.2 Nondimensional buckling load comparison

	ANM	FEM		
		Type **A**	Type **B**	Type **C**
M_{cr}/M_{crANM}	1	0.991	1.001	0.991

(Fig. 4.13) in the form of the maximum deflection of the compressed wall of the girder as a function of the dynamic load factor $DLF = M_a/M_{cr}$, defined as a pulse amplitude of the applied loading divided by the static buckling load M_{cr}.

As can be seen from the curves presented in Fig. 4.13, considerable discrepancies in the results have been obtained with both methods. The differences increase with an increasing dynamic load factor value, which for a higher load lead to larger deformations. The applied boundary conditions are much more significant than for small deformations. Differences in the obtained results mean that the boundary conditions were not properly chosen, which can be confirmed after a closer examination of possible displacements of loaded girder edges. The end section of the bent girder rotates around the neutral axis, and therefore the edges of the upper and lower walls cannot only move along the beam axis but also in the direction normal to the surface of the flanges. Such movements are allowed in the prebuckling state in the analytical-numerical method, however are not possible in the finite element model (Fig. 4.9). Accordingly, the boundary conditions **A** are disqualified and a further analysis was performed for comparison of the two other ways of support (case **B**—Fig. 4.10 and case **C**—Fig. 4.11). As is well visible in Figs. 4.10 and 4.11, the boundary conditions **B** and **C** allow for the necessary movement of ends of the girder subjected to the bending moment.

Analysing the results presented in Fig. 4.13, one can conclude that the best boundary conditions allowing to map and verify the model assumed in the analytical-numerical method are conditions **C** (Fig. 4.11).

Comparing the results of the ANM and the FEM with **A** boundary conditions, it can be seen that the deflection differences increase with an increasing DLF, which means that the boundary conditions make the model stiffer, especially for large deformations. Also, the curve obtained for the **B**-type boundary conditions is far

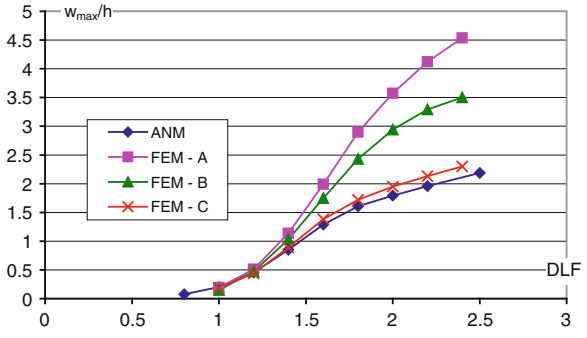

Fig. 4.13 Dimensionless deflection versus DLF for different types of the boundary conditions assumed in the FEM and the ANM

from the curve of the analytical-numerical method. Beam elements in the model **B** do not have an infinite stiffness and, therefore, cannot ensure that the ending cross-section remains flat and the loaded edges of the walls remain straight. The **C**-type boundary conditions allow for free rotation of the final section (which remains flat) around the neutral axis. Thus, for a further finite element analysis (numerical experiment) of girders subjected to bending, the **C**-type boundary conditions are adopted (Fig. 4.11).

Therefore, for all columns with closed cross-sections subject to compression, in which the global mode was taken into consideration, the boundary conditions analogical to the **C**-type were assumed. A similar analysis as the one described above may be carried out for the beam-column with an open cross-section for which the boundary conditions in loaded ends were assumed according to the description presented in Fig. 4.14.

Figure 4.14 shows one example of a column with an open cross-section. For other types of open cross-sections, the boundary conditions were assumed by analogy. It was assumed that bending (the flexural buckling mode) occurred around the axis for which the second moment of area is the smallest, thus the FEM model was prepared in such a way that nodes in which the displacement in the *y* direction was set to zero (Fig. 4.14) were on the neutral axis of ending sections. Straightness of the loaded edges of the considered beam-column is provided by requiring equal displacements of all nodes lying on the edge of the beam-column in the direction normal to its walls. To ensure that deformations are compatible with the deflection in bending (the global flexural buckling mode), the edges normal to the neutral axis remained straight in the plane containing the wall of the column. In addition, for all nodes lying on those edges, the constant rotation around the axis parallel to the axis of the neutral section was presupposed.

When the compressed column was analysed, a compression force or a uniform stress distribution with additional conditions for the uniform edge displacement was assumed. In other cases of load (pure bending or bending with compression),

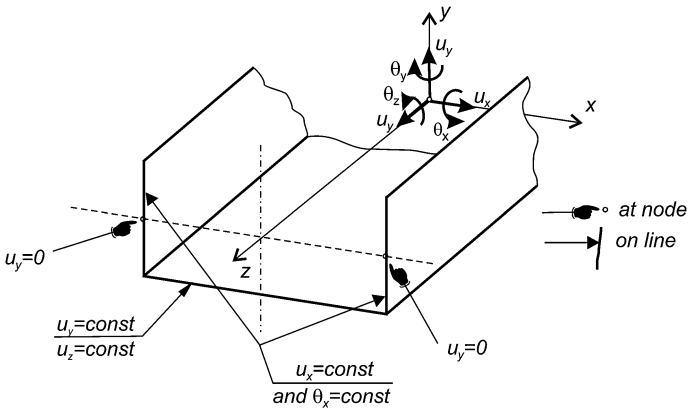

Fig. 4.14 Assumed boundary conditions—an example for a channel cross-section

the stress distribution corresponding to a given load was assumed. The stress distribution was modelled in the form of the pressure distribution acting along the loaded edges of the structure. An exemplary model of load corresponding to pure bending is presented in Fig. 4.15.

It should be noted that the assumed load is nonconservative—pressure is always perpendicular to the area to which it is applied. Let us check what an influence of the assumed model, i.e., the load and the boundary condition, on the results of calculations is. As an example, the channel-shape cross-section profile subjected to pure bending was computed. Four different models denoted as BC-1 to BC-4 were considered, and they are as follows:

BC-1 part (with a length l) of the beam-column between two neighbouring diaphragms, the load is a pressure modelling the bending stress distribution; the boundary condition (displacement set to zero) assumed in neutral axes; in loaded edges of the beam-column, a constant value of displacement in the normal direction to its wall is assumed—Fig. 4.16a;

BC-2 BC-1 model with added constant displacement in the longitudinal direction of the beam-column loaded edges of the web—Fig. 4.16b;

BC-3 considered part of the beam of a length l modelled together with a handle subjected to four-point bending (Fig. 4.17);

BC-4 model three times longer than the considered part of the beam with a diaphragm (Fig. 4.18) and a handle, the whole subjected to four-point bending.

For all the above-mentioned models of static buckling, a modal and nonlinear static analysis was performed. The results of these calculations are presented in Tables 4.3 and 4.4 and in Figs. 4.19 and 4.20.

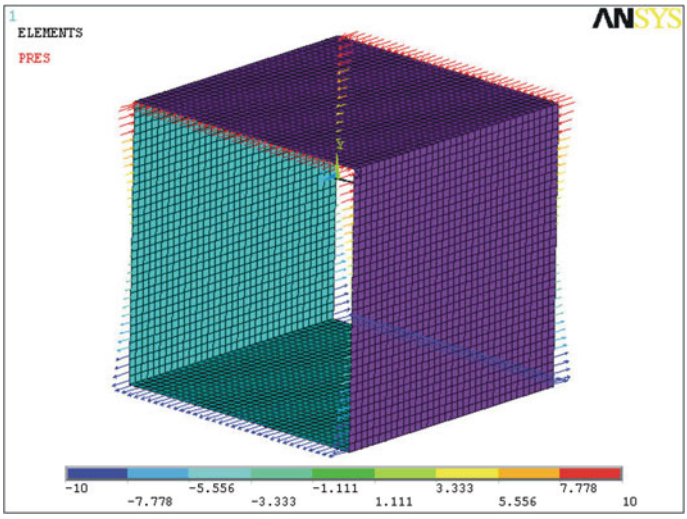

Fig. 4.15 Exemplary load model for a segment of the girder subjected to pure bending

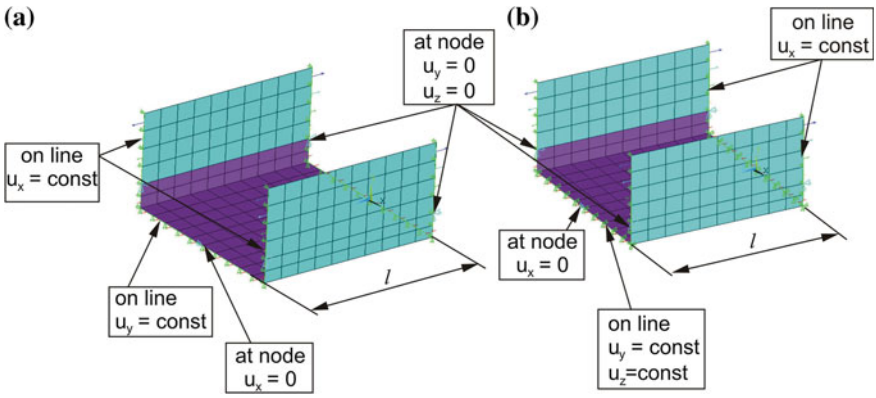

Fig. 4.16 BC-1 (**a**) and BC-2 (**b**) models of channel-shape beam-columns subjected to pure bending

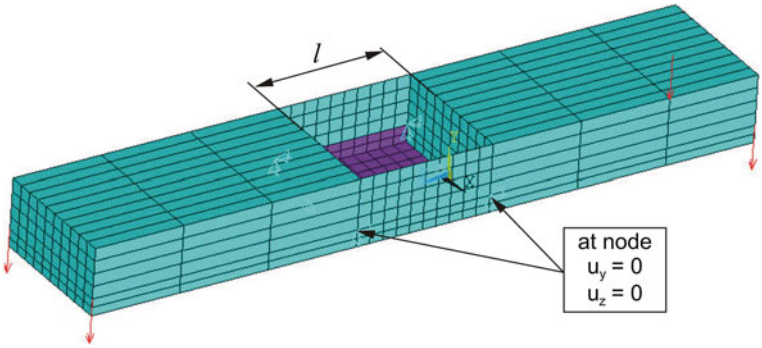

Fig. 4.17 BC-3 model of channel-shape beam-columns subjected to pure bending

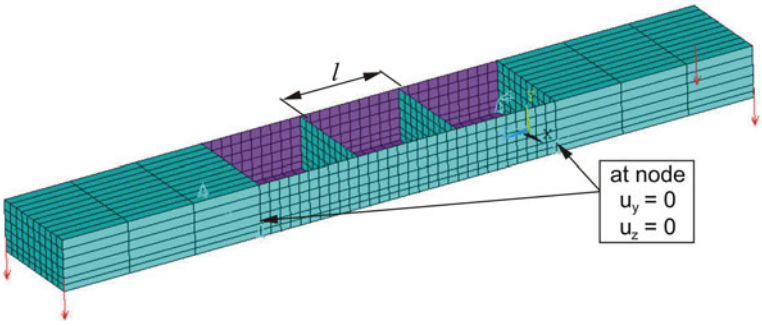

Fig. 4.18 BC-4 model of channel-shape beam-columns subjected to pure bending

Examining the results from the eigenvector analysis (the modal analysis—Table 4.3 and the buckling analysis—Table 4.4), it is well visible that all four considered models of boundary conditions and loads do not play a significant role in the results of calculations—the highest differences are less than 5 %. It means that the simplest models (BC-1 and BC-2) are accurate enough for the static linear analysis. It should be noted that the lowest natural frequencies and the corresponding modal modes for the model denoted as BC-4 are different than for BC-1 and BC-2. The modal mode differences are shown in Fig. 4.19. As can be seen in Fig. 4.19, the first modal mode obtained using the BC-4 model has a global character (Fig 4.19b). Due to these differences, in Table 4.3 only the corresponding modal modes are compared (for example, the first from BC-1 presented in Fig. 4.19a with the third one from BC-4 presented in Fig. 4.19c).

Comparing the results of the nonlinear buckling analysis, it is clear that the considered models of boundary conditions and loads have a significant impact on the structure work in the postbuckling state (Figs. 4.20 and 4.21). Some similarities can be seen when the postbuckling behaviour for the models denoted as BC-2 and BC-4 is compared. The first model denoted as BC-1 is too 'weak'. The lack of the straightness assumption for the loaded web edge leads to a reduction in its stiffness. The model designated as BC-3 is too 'stiff' due to the close box neighbourhood to the considered beam-column part and a much stiffer handle. To be sure which model of load and boundary conditions is correct, experimental tests should be performed.

The next considered case is a girder subjected to torsion. To introduce the load causing twist, one end of the girder was restrained (for all nodes, three perpendicular displacements were set to zero) and two pairs of forces were applied to the second end (Fig. 4.22). Such an assumption leads to a deformation on the not restrained end of the girder and to a not natural stress concentration in the places where the forces are applied (Fig. 4.23).

Table 4.3 Natural frequencies for different models of load and boundary conditions

Length l (mm)	Natural frequencies f (Hz)				Differences[a] (%)
	BC-1	BC-2	BC-3	BC-4	
40	1,117	1,117	1,118	1,135	1
50	836	836	836	850	2
60	678	678	678	690	2
70	579.4	579.4	580	573	1
80	513	513	513	516	1
90	466	466	466	469	1
100	431.3	431.3	431	434	1
150	343.8	343.8	344	345	0
200	310	310	311	310	0
250	293.5	293.5	295	287	3

[a] Differences calculated between the minimal and maximal value divided by the maximal value

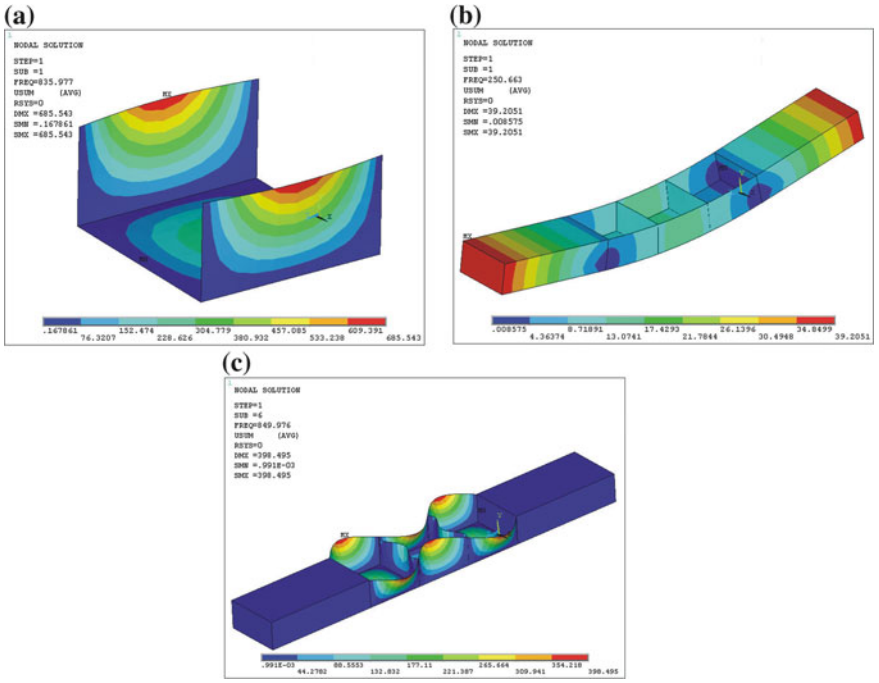

Fig. 4.19 First modal mode for BC-2 (**a**) and BC-4 (**b**) models of the beam-column with the length $l = 50$ mm

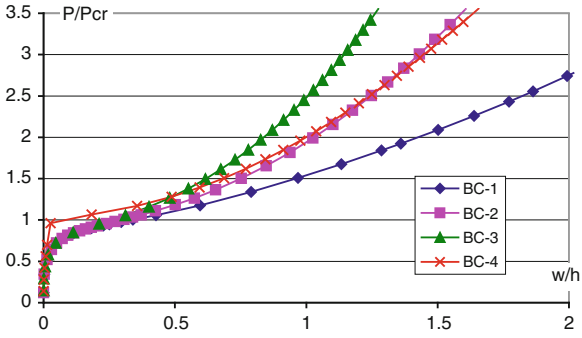

Fig. 4.20 Postbuckling equilibrium path for the channel-shape beam-column of the length $l = 50$ mm

To prevent a stress concentration at loaded points and a deformation of the shape of the one end of the girder, the front panel 10 times thicker than the girder wall thickness (Fig. 4.24) was introduced.

The proposed model can be employed in the analysis of girders subjected to torsion because there are no unexpected deformations—both ends of the girder after loading remain the same square shape (Fig. 4.25).

The most difficult arrangement of the boundary condition was for the girders subjected to a combined load—a simultaneously applied bending moment and a

Table 4.4 Critical bending moment for different models of boundary conditions

Length l (mm)	Buckling mode (m)	Critical bending moment M_{cr} (Nm)				Differences[a] (%)
		BC-1	BC-2	BC-3	BC-4	
40	1	52	52	51	53	4
50	1	55	55	55	57	3
60	1	63	63	62	65	4
	2	57	57	58	58	3
70	1	73	74	73	76	3
	2	53	53	53	54	2
80	1	86	86	87	88	2
	2	52	52	53	53	3
90	1	101	101	102	104	2
	2	53	53	54	54	2
100	1	118	118	120	121	2
	3	54	54	55	55	2
150	1	226	226	233	233	3
	4	52	52	53	54	3
200	1	359	360	372	374	4
	5	52	52	53	53	2
250	1	493	495	516	514	4
	6	52	52	53	55	5

[a] Differences calculated between the minimal and maximal value divided by the maximal value

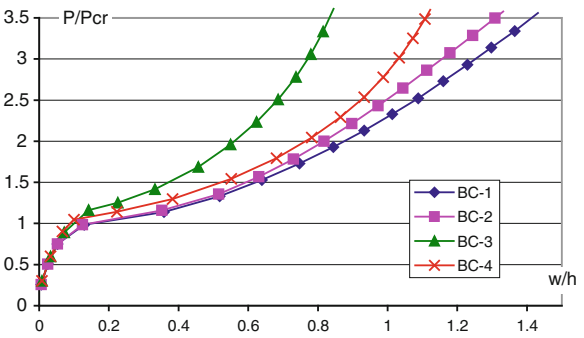

Fig. 4.21 Postbuckling equilibrium path for the channel-shape beam-column of the length $l = 200$ mm

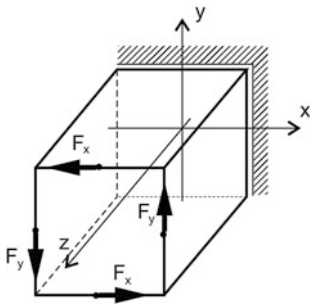

Fig. 4.22 Model of the boundary conditions and the load for the analysed girder

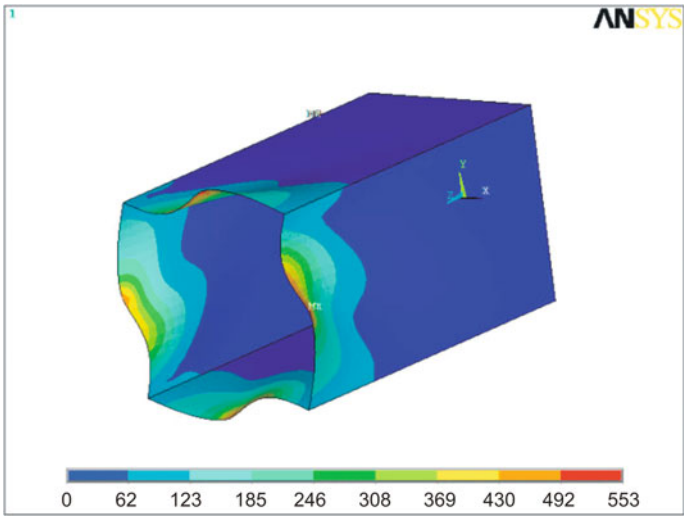

Fig. 4.23 Deformation and the equivalent stress distribution for the first model

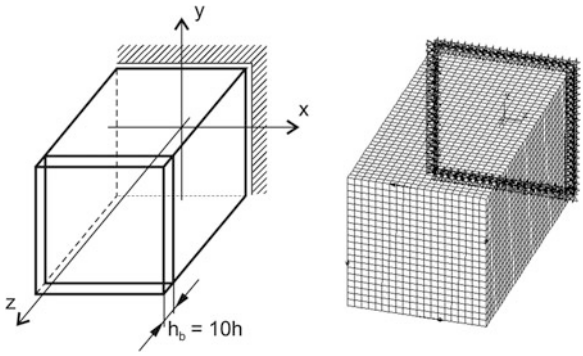

Fig. 4.24 Models with a solution preventing deformation and stress concentrations

torque. The assumed boundary condition cannot block displacements corresponding to a given type of load and prevent unexpected stress concentrations (i.e., the stress concentration in the corners on the plane where the loads are applied). Two different models were considered (Fig. 4.26). In order to assure the linearity of loaded edges, in the first model two plates of relatively high stiffness were added to the ends of the girder (Fig. 4.26a). In the second model, the same linearity of the loaded edges was obtained by an application of beam elements (Fig. 4.26b).

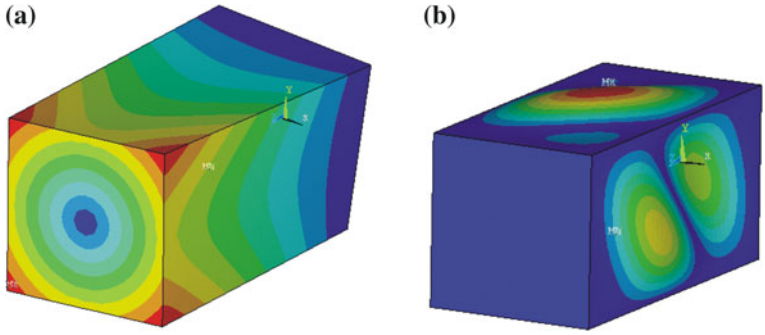

Fig. 4.25 Results of static (**a**) and buckling (**b**) analyses for the model with a front panel

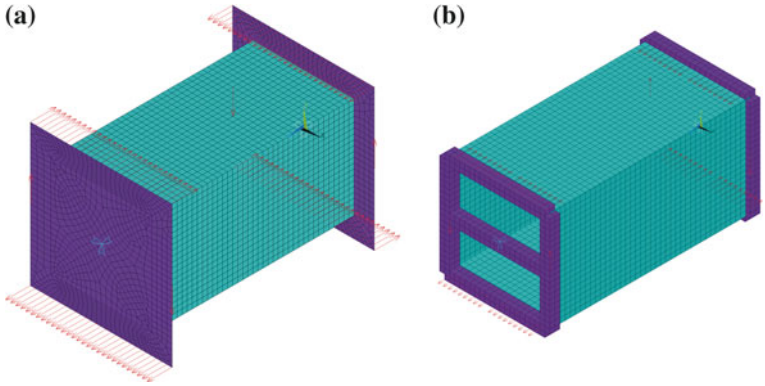

Fig. 4.26 FEM models: **a** plate model (Model 1), **b** beam model (Model 2)

References

1. ANSYS 11.1 html online documentation, SAS IP, Inc, 2007
2. Bathe KJ (1996) Finite element procedures. Prentice-Hall, Englewood Cliffs
3. Chroscielewski J, Makowski J, Pietraszkiewicz W (2004) Statyka i dynamika powlok wieloplatowych: nieliniowa teoria i metoda elementow skonczonych. IPPT PAN, Warsaw
4. Courant R (1943) Variational methods for the solution of problems of equilibrium and vibrations. Bull Am Math Soc 49:1–23
5. Crisfield MA (1997) Non-linear finite element analysis of solids and structures. John Wiley & Sons, Inc, New York
6. Forde WRB, Stiemer SF (1987) Improved arc length orthogonality methods for nonlinear finite element analysis. Comput Struct 27(5):625–630
7. Fortuna Z, Macukow B, Wąsowski J (2006) Metody Numeryczne. WNT, Warsaw
8. Guarracino F (2001) The elastic-plastic behaviour of cylindrical tubes under bending: finite elements analyses, experimental data and theoretical consideration. In: Zaras J, Kowal-Michalska K, Rhodes J (eds) Proceedings of international workshop on the application of finite element method to the analysis of thin-walled structures, addendum to proceedings of third international conference of thin-walled structures, Cracow, pp 5–14

9. Guarracino F (2003) On the analysis of cylindrical tubes under flexure: theoretical formulations, experimental data and finite element analyses. Thin Wall Struct 41:127–147
10. Desai CS, Siriwardane HJ (1980) An introduction to finite element computations. In: Hinton E, Owen DR (eds) Pineridge Press, Swansea
11. Kolakowski Z, Kubiak T (2004) Multiple interaction of dynamic buckling modes in thin-walled members subjected in-plane pulse loading. In: Proceedings of 4th international conference on coupled instabilities in metal structure, Rome, Italy, 27–29 September 2004
12. Kolakowski Z, Kubiak T (2005) Load-carrying capacity of thin-walled composite structures. Compos Struct 67:417–426
13. Kounadis AN, Gantes C, Simitses G (1997) Nonlinear dynamic buckling of multi-dof structural dissipative system under impact loading. Int J Impact Eng 19(1):63–80
14. Krolak M, Mania RJ (eds) (2011) Static, dynamic and stability of structures. Vol. 1: Stability of thin-walled plate structures. A series of monographs. Technical University of Lodz Press, Lodz
15. Kubiak T (2005) Dynamic buckling of thin-walled composite plates with varying widthwise material properties. Int J Solids Struct 45:5555–5567
16. Kubiak T (2005) Dynamic buckling of thin-walled girders with channel cross-section. VDI-Berichte 1899:69–78
17. Kubiak T (2005) Dynamic buckling of thin composite plates. In: Proceedings IUTAM symposium on multiscale modelling and fracture processes in composite materials, Springer, pp 123–130
18. Kubiak T (2005) Wyboczenie dynamiczne cienkosciennych dzwigarow kompozytowych. In: Proceedings of IX-th scientific-technical conference FEM software in computer aided analysis, design and manufacturing, Gizycko, Poland, pp 89–96
19. Kubiak T (2007) Metoda elementow skonczonych jako eksperyment numeryczny statecznosci dzwigarow cienkosciennych obciazonych statycznie i dynamicznie. In: Niezgoda T (ed) Numerical analysis of selected problem in mechanics. Military University of Technology Press, Warsaw, pp 209–228
20. MacNeal RH, Harder RL (1988) A refined four-noded membrane element with rotational degrees of freedom. Comput Struct 28(1):75–84
21. Reddy JN (2004) An introduction to nonlinear finite element analysis. Oxford University Press, New York
22. Riks E (1979) An incremental approach to the solution of snapping and buckling problems. Int J Solids Struct 15:529–551
23. Szmelter J, Dacko M, Dobrocinski S, Wieczorek M (1973) Komputerowe programy metody elementow skonczonych. Arkady, Warszawa
24. Szmelter J, Dacko M, Dobrociński S, Wieczorek M (1979) Metoda elementow skonczonych w statyce konstrukcji. Arkady, Warszawa
25. Timoshenko SP, Gere JM (1961) Theory of elastic stability. McGraw-Hill, New York
26. Turner MJ, Clough RW, Martin HC, Topp LJ (1956) Stiffness and deflection analysis of complex structures. J Aero Sci 23(9):805–823
27. Washizu K (1974) Variational method in elasticity and plasticity. Pergamon Press, Oxford
28. Zienkiewicz OC (1971) The finite element method in engineering science. McGraw-Hill, London
29. Zienkiewicz OC, Cheung YK (1967) The finite element method in structural and continuum mechanics: numerical solution of problems in structural and continuum mechanics. McGraw-Hill, London
30. Zienkiewicz OC, Taylor RL (2000) The finite element method. Butterworth-Heinemann, Oxford